Stem Cell Reports
Article

ISSCR

OPEN ACCESS

Identification of Drugs that Regulate Dermal Stem Cells and Enhance Skin Repair

Sibel Naska,[1,7,8] Scott A. Yuzwa,[1,7] Adam P.W. Johnston,[1] Smitha Paul,[1] Kristen M. Smith,[1,9] Maryline Paris,[1,10] Michael V. Sefton,[6] Alessandro Datti,[2,3] Freda D. Miller,[1,4,5,*] and David R. Kaplan[1,4,*]

[1]Program in Neurosciences and Mental Health, Hospital for Sick Children, Toronto, ON M5G 0A4, Canada
[2]S.M.A.R.T. Laboratory for High-Throughput Screening Programs, Lunenfeld-Tanenbaum Research Institute, Mount Sinai Hospital, Toronto, ON M5G 1X5, Canada
[3]Department of Agricultural, Food, and Environmental Sciences, University of Perugia, 06121 Perugia, Italy
[4]Department of Molecular Genetics
[5]Department of Physiology
[6]Institute of Biomaterials and Biomedical Engineering
University of Toronto, Toronto, ON M5G 1X5, Canada
[7]Co-first author
[8]Present address: Ontario Brain Institute, Suite 1618, 438 University Avenue, Toronto, ON M5G 2K8, Canada
[9]Present address: Bionomics, Inc, 11585 Sorrento Valley Road, San Diego, CA 92121, USA
[10]Present address: L'Oreal Research and Innovation, 1 Avenue Eugène Schueller, Aulnay-sous-Bois 93600, France
*Correspondence: fredam@sickkids.ca (F.D.M.), dkaplan@sickkids.ca (D.R.K.)
http://dx.doi.org/10.1016/j.stemcr.2015.12.002
This is an open access article under the CC BY-NC-ND license (http://creativecommons.org/licenses/by-nc-nd/4.0/).

SUMMARY

Here, we asked whether we could identify pharmacological agents that enhance endogenous stem cell function to promote skin repair, focusing on skin-derived precursors (SKPs), a dermal precursor cell population. Libraries of compounds already used in humans were screened for their ability to enhance the self-renewal of human and rodent SKPs. We identified and validated five such compounds, and showed that two of them, alprostadil and trimebutine maleate, enhanced the repair of full thickness skin wounds in middle-aged mice. Moreover, SKPs isolated from drug-treated skin displayed long-term increases in self-renewal when cultured in basal growth medium without drugs. Both alprostadil and trimebutine maleate likely mediated increases in SKP self-renewal by moderate hyperactivation of the MEK-ERK pathway. These findings identify candidates for potential clinical use in human skin repair, and provide support for the idea that pharmacological activation of endogenous tissue precursors represents a viable therapeutic strategy.

INTRODUCTION

Advances in adult tissue stem cell biology have led to the idea that pharmacological activation of resident stem cells might represent a therapeutic strategy for tissue repair (Miller and Kaplan, 2012). Indeed, pharmacological candidates that regulate tissue stem cells have been identified including, for example, metformin for neural precursors (Wang et al., 2012; Dadwal et al., 2015) and StemRegenin 1 for primary human hematopoietic stem cells (Boitano et al., 2010). Here, we asked whether this is a viable strategy for skin repair. Skin is a complex tissue with many endogenous tissue stem cells. These include epidermal stem cells (Hsu et al., 2014) and a population of dermal stem cells called skin-derived precursors (SKPs) (Toma et al., 2001, 2005). Cultured SKPs clonally generate mesenchymal progeny like dermal fibroblasts and adipocytes, and peripheral neural progeny like Schwann cells, consistent with the finding that they derive from both neural crest and mesodermal origins (Fernandes et al., 2004; McKenzie et al., 2006; Jinno et al., 2010; Krause et al., 2014), like the dermis itself. With regard to their in vivo function, cultured SKPs can clonally reconstitute the dermis and induce hair follicle morphogenesis (Biernaskie et al., 2009), suggesting key roles for the endogenous precursors in dermal maintenance and hair follicle biology.

Here, we have tested the idea that increasing the number and/or self-renewal of endogenous SKPs would enhance skin repair. To do so, we screened libraries of compounds that are used clinically in humans, looking for drugs that enhance SKP self-renewal. We identified two compounds, alprostadil and trimebutine maleate (TM), that increased SKP self-renewal, likely by activating the MEK-ERK pathway. Both compounds enhanced wound healing when applied topically. These findings provide proof of principle for the idea that compounds that regulate SKPs in culture have therapeutic efficacy in vivo, and identify potential drug candidates that can be repositioned for use in humans.

RESULTS

Screens to Identify Compounds that Enhance Human and Rodent SKP Self-Renewal and Proliferation

We performed high-throughput proliferation screens using primary human foreskin SKPs and neonatal rat dorsal SKPs grown as spheres in serum-free growth medium containing

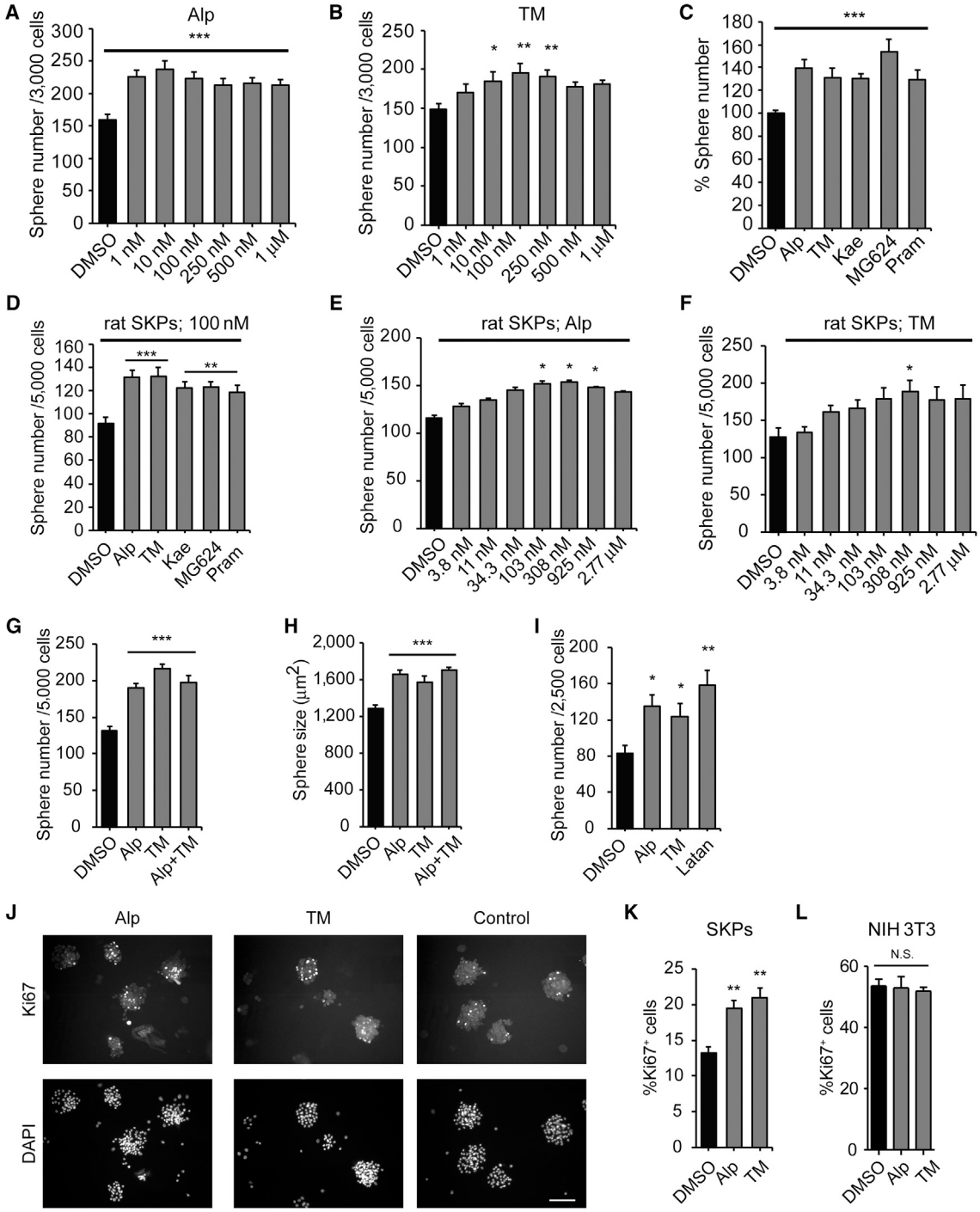

Figure 1. Identification of Compounds that Enhance Self-Renewal and Proliferation of Cultured SKPs

(A–C) Number of SKP spheres generated from secondary human SKPs grown for 7 days in varying concentrations of alprostadil (Alp) (A) or TM (B) or in 100 nM alprostadil, TM, kaempferol (Kae), MG-624, or pramoxine (Pram) (C). In (C) numbers are expressed relative to DMSO alone.

(D–F) Number of SKP spheres generated from secondary neonatal rat SKPs grown for 7 days in 100 nM of each of the five drugs (D), or in varying concentrations of alprostadil (E) or TM (F).

(G and H) Number (G) and size (H) of rat SKP spheres generated over 7 days in 100 nM alprostadil, TM, or both.

(I) Number of rat SKP spheres generated in 14-day clonal methylcellulose assays with 100 nM alprostadil, TM, or latanoprost (Latan).

(legend continued on next page)

40 ng/ml fibroblast growth factor 2 (FGF2) and 20 ng/ml epidermal growth factor (EGF). This study was approved by the Hospital for Sick Children Animal Care Committee in accordance with CCAC guidelines, and for human tissues and cells, with the approval of the Research Ethics Board of the Hospital for Sick Children. We chose 3,000 human and 5,000 rat SKP cells per well as optimal cell numbers by robotically plating cells in 96-well plates, adding alamarBlue at 30 hr, and assessing its reduction 24 hr later as a measure of cell metabolic activity (Figure S1A) (Smith et al., 2010). We then performed two sets of screens. In one, spheres from four independent human SKP lines (Smith et al., 2010) were dissociated and treated with the Prestwick library of 1,120 compounds (primarily marketed drugs), and the LOPAC-Sigma library of 1,280 compounds with proven biological activity at 1 or 5 μM. In the second, rat or human SKPs were treated with the NIH Clinical Collection library of 446 highly drug-like compounds with known human safety profiles.

Hits were defined as (1) compounds with signals (B scores) shifted at least three SDs (99.73% confidence interval) from the mean of the general sample population (Figures S1B and S1C), or (2) compounds with a 20% or more increase in alamarBlue values relative to controls in at least three different human SKP lines. For secondary screens, we dissociated human SKPs from at least three independent lines, plated them in growth medium, added drugs on days 1 and 4, and on day 7 quantified spheres as an index of self-renewal. This analysis (Figures 1A and 1B; Figures S1D–S1F) confirmed five of the potential hits: alprostadil (prostaglandin E1 [PGE1]), used for erectile dysfunction (Hanchanale and Eardley, 2014); TM, a weak opioid receptor agonist and spasmolytic (Delvaux and Wingate, 1997); the natural flavonoid kaempferol (Calderón-Montaño et al., 2011); MG-624, an α7-nicotinic acetylcholine receptor antagonist used for postoperative vomiting (Gotti et al., 1998); and pramoxine, a local anesthetic (Fisher, 1998). All compounds have been used in humans, and all but MG-624 have been used topically. Three compounds, alprostadil, TM, and kaempferol, enhanced sphere number at doses as low as 1–10 nM (Figures 1A and 1B; Figure S1D), while others had effects at higher concentrations (Figures S1E and S1F). None of the compounds had toxic effects at concentrations up to 1 μM except for MG-624 (Figure S1E). A direct comparison showed that at 100 nM, all the drugs promoted sphere formation to approximately the same extent (Figure 1C). Similar results were obtained in secondary sphere formation assays with neonatal rat SKPs (Figure 1D).

We chose alprostadil and TM for more detailed characterization, since (1) they were efficacious in secondary screens, (2) they are used topically in humans, and (3) SKPs express the mRNAs encoding the EP(1–4) prostanoid receptors for alprostadil and the mu and kappa-opioid receptors for TM (data not shown). Initially, we performed dose-response curves with rat SKPs. Sphere numbers increased in a dose-dependent fashion to a maximum at 103–308 nM for alprostadil and 308 nM for TM (Figures 1E and 1F). Second, we added 100 nM of the drugs together or alone in sphere formation assays. Each drug alone increased sphere number and size (the latter a surrogate measure of proliferation), with no further increase with both (Figures 1G and 1H), suggesting that they might act via similar mechanisms. Third, we measured self-renewal using a colony formation assay in which rat SKPs were plated at clonal density (2.5 cells/μl) in medium containing 1.6% methylcellulose. For comparison, we also analyzed latanoprost, a prostaglandin (PGF2) that is bioactive in rodent and human skin (Sasaki et al., 2005). Clonal sphere numbers were significantly increased by all three drugs at 14 days (Figure 1I). Finally, we directly measured proliferation; rat SKPs were cultured for 3–4 days, treated with drugs daily for a further 2 days, and immunostained for the proliferation marker Ki67. Both drugs increased Ki67-positive sphere cells by approximately 60% (Figures 1J and 1K). These drugs are not general mitogens, since Ki67-positive NIH 3T3 cells were unaffected in similar assays (Figure 1L). Thus, alprostadil and TM increase SKP proliferation and self-renewal.

Alprostadil and TM Enhance Skin Repair in Middle-Aged Mice

To ask whether alprostadil or TM promoted skin repair, we performed 6-mm diameter full thickness punch wounds on middle-aged (9 months old) mice, as we have previously described (Johnston et al., 2013), and applied the drugs daily for 9 days around the injury site, using 100 μM drug in a propylene glycol-ethanol-water mixture that enables

(J and K) Secondary rat SKP spheres were grown for 4 days, and 100 nM alprostadil or TM was added for two additional days. (J) shows spheres immunostained for Ki67 (top) and counterstained with DAPI to show nuclei (bottom). (K) shows the percentage of Ki67-positive cells. Scale bar represents 100 μm.

(L) NIH 3T3 cells were treated for 24 hr with 100 nM alprostadil or TM, immunostained for Ki67, and the percentage of positive cells determined. N.S., not significant.

In all panels, results were pooled from 3 to 4 independent experiments with, in the human experiments, 3–4 different human SKP lines. Error bars indicate SEM, and in all cases *$p < 0.05$, **$p < 0.01$, ***$p < 0.001$, one-way ANOVA with multiple comparison post hoc tests. See also Figure S1.

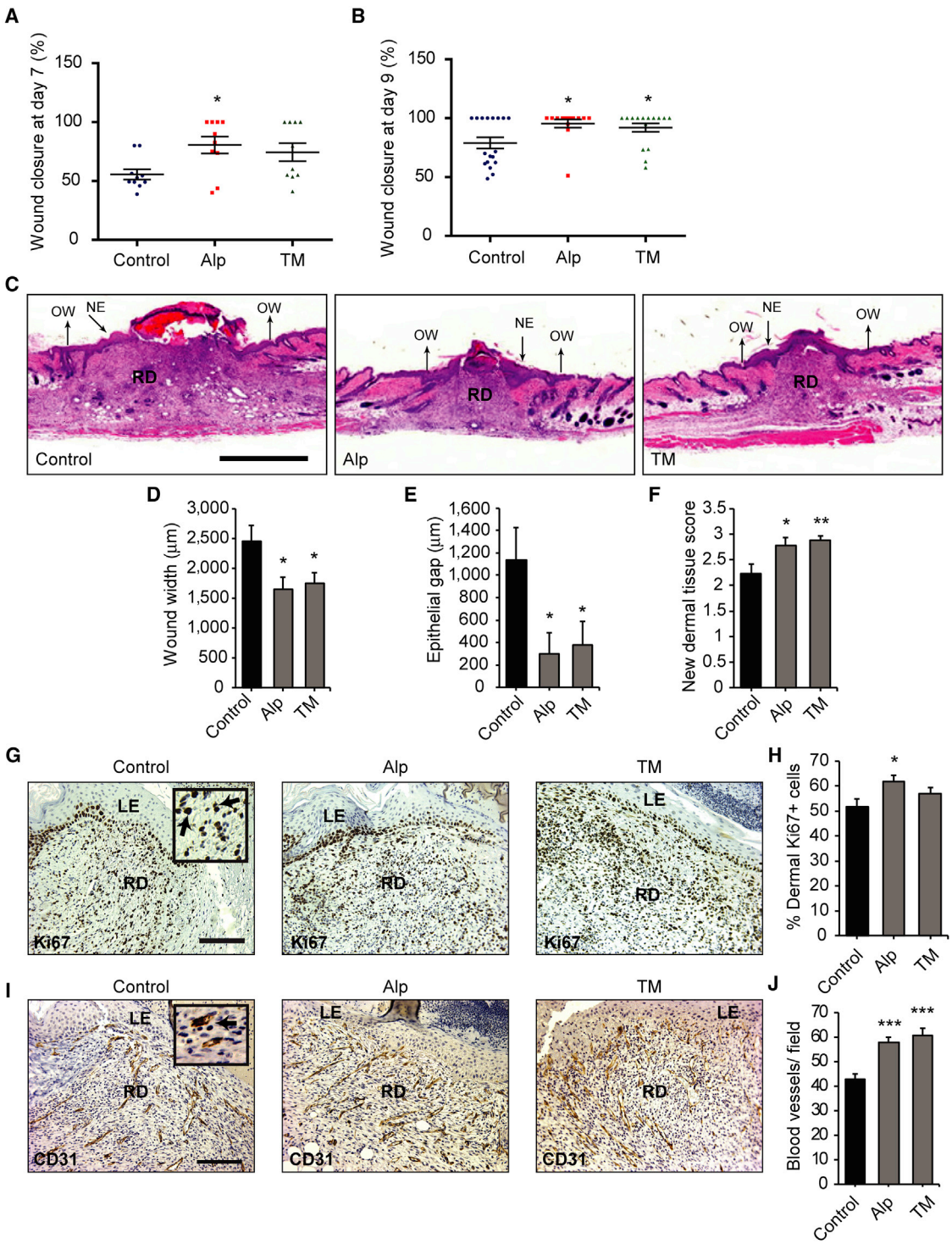

Figure 2. Topical Alprostadil or TM Promotes Skin Repair in Middle-Aged Mice

(A and B) Scatterplots showing wound closure at 7 days (A) and 9 days (B) after injury for 9-month-old mice treated daily with alprostadil (Alp), TM, or vehicle alone (Control). n = 10 or 14 mice per group, from three independent experiments.

(C–F) H&E-stained sections through the center of the wound bed 9 days after injury (C) were analyzed for wound width (D), epithelial gap (E), and new dermal tissue (F). n = 18, 14, and 17, vehicle-, alprostadil-, and TM-treated mice total, from three independent experiments. NE indicates the new epithelium, RD the regenerating dermis, and OW the borders of the wound. Scale bar represents 1 mm.

(legend continued on next page)

dermal penetration (Tata et al., 1995). Wound closure was significantly accelerated in drug-treated mice. On day 7, almost half of the alprostadil- or TM-treated mice were fully healed, as opposed to none of the vehicle-treated controls (Figure 2A). By day 9, 70%–78% (11 of 14 for alprostadil and 10 of 14 for TM) of drug-treated mice were healed compared with 44% (8 of 18) of the vehicle-treated mice (Figure 2B).

Morphometric analyses of H&E-stained paraffin sections from the central portion of the wound bed on day 9 (Figure 2C) confirmed these results. Wound width (Figure 2D) and epithelial gap (Figure 2E) were both significantly smaller in alprostadil- or TM-treated mice. Dermal tissue regeneration was also enhanced, with a thicker layer of new dermal tissue (Figures 2C and 2F). In alprostadil-treated mice, this coincided with increased Ki67-positive proliferating dermal cells at the leading edge of the newly formed dermis 7 days after injury (Figures 2G and 2H). Treatment with alprostadil or TM also increased CD31-positive blood vessels in the same region (Figures 2I and 2J).

Topical Treatment of Mouse Skin with Alprostadil or TM in Vivo Causes Long-Term Enhancement of the Self-Renewal of SKPs Cultured from Treated Skin in the Absence of Drugs

These data indicate that alprostadil and TM enhance SKPs self-renewal in culture and promote skin repair in vivo. To provide a link between these two activities, we performed punch wounds on 9-month-old mice, treated them with alprostadil, TM, or vehicle daily for 7 days, and then cultured SKPs from the regenerating skin without added drugs. For comparison, we analyzed uninjured mice following topical drug application for 7 days. The number and size of secondary SKP spheres were increased when they were isolated from either injured or uninjured drug-treated skin (Figures 3A–3D; Figure S2A), indicating that alprostadil and TM somehow regulated endogenous dermal precursors to affect their long-term self-renewal even when they were isolated and cultured without these drugs.

To ask about the nature of the drug-induced change(s), we performed transcriptome analysis on the different secondary SKP sphere populations, isolating RNA from three independent biological replicates of each and using Affymetrix GeneChip Mouse Gene 2.0 ST Arrays. Unbiased hierarchical clustering (using the complete linkage method) of a Euclidean distance matrix of $\log_2$ normalized expression data demonstrated that, while the different biological replicates for each treatment population clustered together, the different populations were all highly similar to each other (Figure 3E). Intriguingly, the clustering also showed that SKPs from alprostadil- and TM-treated injured skin were more similar to each other and to those from uninjured skin than to SKPs from vehicle-treated injured skin, potentially reflecting the accelerated wound healing caused by these two drugs.

The conclusion that these different SKP populations were all similar was further supported by differential gene expression analysis with the limma bioconductor package (Ritchie et al., 2015). Only 165 and 291 annotated genes were differentially expressed in SKPs from alprostadil and TM versus vehicle-treated injured skin, respectively ($p < 0.01$ for both comparisons) (Figure 3F). These differentially expressed genes were largely non-overlapping (Tables S1 and S2), with only 21 shared between the alprostadil and TM groups (Figure S2B). Thus, transcriptionally similar SKP populations are present from treated or untreated skin, and somehow the drug treatments enhance their long-term self-renewal when these SKPs are cultured in vitro.

Alprostadil and TM Regulate Genes in Cultured SKPs that Are Associated with Cell Proliferation and the MAP Kinase Pathway

One potential explanation for the modest gene expression changes observed in the long-term experiments was the long lag time between drug exposure and analysis. We therefore performed acute drug exposure experiments. Primary rat SKPs were passaged, acutely treated with drugs for 24 hr, and analyzed via microarrays as for the long-term experiments. This analysis identified 457 and 545 differentially expressed genes in the pairwise comparisons of control versus alprostadil or TM treatment, respectively ($p < 0.01$ for both comparisons) (Tables S3 and S4). The changes were generally of higher magnitude for alprostadil than for TM (Figure 3G), but more than half of the significantly changed genes (295) were shared between the two groups (Figure 3H; Table S5). In addition, of the top 50 differentially expressed genes in the two pairwise comparisons (defined as highest significance; Table S6 and S7), 23 were

(G–J) Sections from the center of the wound bed of mice 7 days after injury were immunostained for Ki67 (G and H) or CD31 (I and J), counterstained with hematoxylin, and analyzed for the percentage of Ki67-positive cells (H) or the relative number of CD31-positive blood vessels (J) at the leading edge of the regenerating dermis. n = at least nine mice per group in (H) and three per group in (J). Insets in (G and I) show higher magnification images, with arrows denoting positive cells (black or dark brown). LE indicates the leading edge of the new epidermis, and RD the regenerating dermis. Scale bar represents 125 μm.

Error bars indicate SEM, and in all cases *$p < 0.05$, **$p < 0.01$, ***$p < 0.001$, one-way ANOVA with multiple comparison post hoc tests except for (E), where comparisons were made by pairwise Student's t tests.

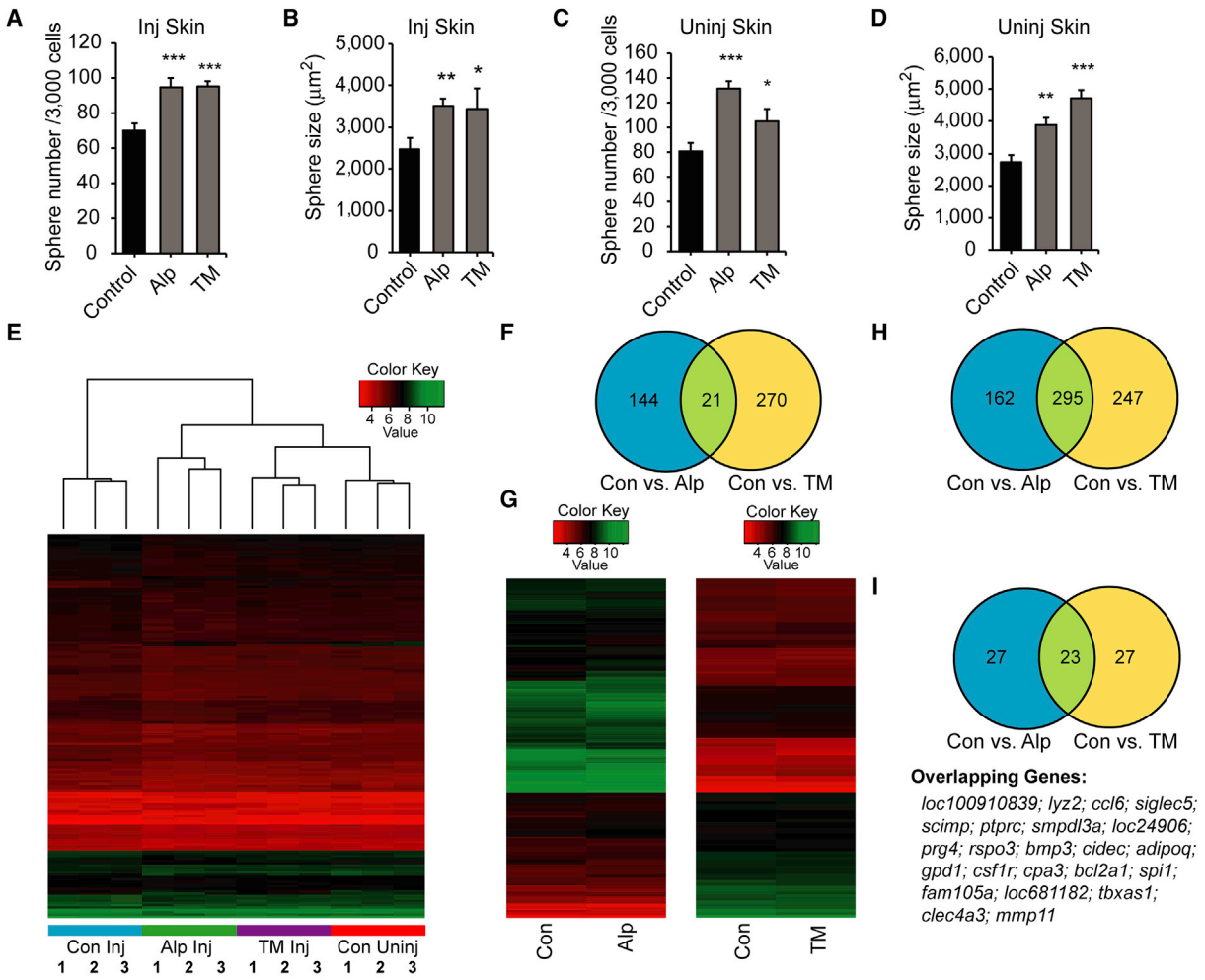

J

GO ID (Biological Process)	Ctrl vs. Alp (P-value)	Ctrl Vs. TM (P-value)	Term Description
GO:0008283	3.29E-11	3.60E-10	cell proliferation
GO:0008284	1.14E-10	1.13E-07	positive regulation of cell proliferation
GO:0042127	2.54E-10	1.82E-09	regulation of cell proliferation

K

GO ID (Biological Process)	Ctrl vs. Alp (P-value)	Ctrl Vs. TM (P-value)	Term Description
GO:0000165	5.12E-08	6.94E-05	MAPK cascade
GO:0043410	7.29E-08	0.000264	positive regulation of MAPK cascade
GO:0043408	9.80E-08	0.000112	regulation of MAPK cascade
GO:0070371	1.16E-07	1.76E-05	ERK1 and ERK2 cascade
GO:0070372	1.62E-07	2.34E-05	regulation of ERK1 and ERK2 cascade
GO:0043405	1.86E-06	0.000167	regulation of MAP kinase activity
GO:0070374	3.07E-05	0.000504	positive regulation of ERK1 and ERK2 cascade

Figure 3. Topical Treatment of Mouse Skin with Alprostadil or TM In Vivo Alters the Self-Renewal of SKPs Cultured from the Treated Skin in the Absence of Drug, and Acute Drug Treatment of Cultured SKPs Causes Changes in Gene Expression

(A–D) Primary SKPs were isolated from 9-month-old mice that had received punch wounds (Inj Skin; A and B) or that had intact skin (Uninj Skin; C and D) and that were then treated with topical vehicle (Control), alprostadil (Alp), or TM for 7 days. The primary SKPs were passaged into medium without drugs and the number (A and C) and size (B and D) of secondary spheres were quantified. n = at least three independent experiments each and error bars indicate SEM. *$p < 0.05$, **$p < 0.01$, ***$p < .001$, one-way ANOVA with multiple comparison post hoc tests except for (B), where pairwise comparisons of control versus alprostadil or TM were made with Student's t test.

(E and F) mRNA from secondary SKP spheres generated as in (A–D) were analyzed on Affymetrix GeneChip Mouse Gene 2.0 ST arrays. (E) Heatmap and hierarchical clustering of all the samples based on probesets that differed by $p < 0.01$ (unadjusted) regardless of the fold change when comparing SKPs from vehicle-treated, injured skin versus alprostadil-treated injured skin. Three independent replicates of SKPs from vehicle-treated injured skin (Con Inj), alprostadil- or TM-treated injured skin (Alp Inj or TM Inj), and vehicle-treated uninjured skin (Con Uninj) were compared.

(legend continued on next page)

shared (Figure 3I), suggesting mechanistic convergence between alprostadil and TM.

Gene ontology (GO) enrichment analysis using the GOstats bioconductor package (Falcon and Gentleman, 2007) showed that, consistent with the biological effects of alprostadil and TM, genes associated with cell proliferation were significantly enriched (Figure 3J) for both drugs. Of the genes that were associated with proliferation (Table S8), 25 overlapped between TM and alprostadil, and a number encoded either growth factors (such as *LIF*, *IL6*, and *FGF10*) or growth factor receptors (such as *LIF* and *EGF* receptors). Intriguingly, of all the signaling pathways, GO terms indicating positive regulation of the MAP kinase pathway were most highly enriched for both drugs (Figure 3K; Table S9), suggesting that they might increase SKP self-renewal by activating this pathway.

Alprostadil and TM Likely Regulate SKPs by Stimulating a MEK-ERK Self-Renewal Pathway

On the basis of these findings, we asked whether alprostadil or TM activated the MEK-ERK pathway in cultured SKPs. We cultured dissociated SKPs for 24 hr, added 100 nM alprostadil or TM for 10 min, and performed western blots for phosphorylated, activated ERK1/2. SKPs grown in FGF2 and EGF had basal levels of ERK1/2 phosphorylation that were increased approximately 2-fold by treatment with either drug (Figures 4A and 4B). In contrast, neither drug increased the phosphorylated activated forms of STAT3, GSK3beta, Akt1, or CREB (Figure 4C and S.N., F.D.M., and D.R.K., unpublished data).

We next asked whether MEK-ERK activity was important for SKP self-renewal, using the highly selective MEK1/2 inhibitor trametinib (GSK1120212) (Gilmartin et al., 2011), after first demonstrating that it inhibited basal ERK1/2 phosphorylation in cultured SKPs (Figure 4D). To ask about self-renewal, we used the methylcellulose colony formation assay. Trametinib decreased both the number (Figure 4E) and size (Figure 4F) of clonal spheres grown in FGF2 and EGF. MEK inhibition also decreased SKPs proliferation, as monitored by Ki67 immunostaining of SKP spheres cultured for 48 hr with or without trametinib, but not survival, as monitored by DAPI staining for nuclear morphology (Figures 4G and 4H).

Three lines of evidence indicated that MEK-ERK activity was also important for drug-induced self-renewal. First, trametinib suppressed the ability of alprostadil and TM to increase ERK1/2 phosphorylation in SKPs cultured for 24 hr (Figure 4I). Second, in 7-day sphere assays, inhibition of MEK with 100 nM trametinib robustly decreased sphere number and neither drug could compensate for this decrease (Figure 4J). Third, microarrays showed that trametinib decreased, in part, the downstream gene expression changes seen when SKPs were cultured in TM for 24 hr. Specifically, of the top 50 genes changed by TM treatment, over half (29) had a reduced fold change when trametinib was also included in the cultures (Figure 4K).

DISCUSSION

The experiments presented here identify compounds that promote SKP self-renewal and proliferation in culture, and provide evidence that these compounds activate dermal precursors in vivo to promote skin repair. They also define the MEK-ERK pathway as a key self-renewal pathway for SKPs, and suggest that molecules targeting distinct cell surface receptors enhance self-renewal by converging on this intracellular signaling pathway. These data therefore provide support for the concept that pharmacological activation of endogenous tissue stem cells provides a valid therapeutic approach (Miller and Kaplan, 2012).

How do alprostadil, TM, and SKP growth factors activate the MEK-ERK pathway to enhance SKP proliferation and self-renewal? FGF2 and EGF signal via receptor tyrosine kinases expressed by SKPs, and are well-known activators of the MEK-ERK pathway. Alprostadil (PGE1) binds to the EP1–4 isoforms of the EP family of receptors (Breyer et al., 2001), which are known to stimulate ERK1/2 (Yu et al., 2008). TM binds peripheral mu and kappa-opioid receptors (Kaneto et al., 1990), which also activate ERK1/2 (Gutstein et al., 1997). Thus, three distinct cell surface cues converge

(F) Venn diagram comparing the overlap of genes that differed by $p < 0.01$ (unadjusted) from pairwise comparisons of SKPs from vehicle (Control) versus TM- or alprostadil-treated injured skin.

(G–K) Three independent preparations of primary neonatal rat SKPs were dissociated and cultured for 24 hr in alprostadil, TM, or vehicle (Con), and mRNA was isolated and analyzed on an Affymetrix GeneChip Rat Gene 2.0 ST array. (G) Heatmaps of pairwise comparisons of vehicle versus alprostadil- or TM-treated SKPs showing the average of the raw expression (log_2) data for probesets that differed by $p < 0.01$ (unadjusted) with a fold change of greater than 1.1. (H and I) Venn diagrams comparing the overlap of all genes that differed by $p < 0.01$ (unadjusted) (H) or the top 50 most significantly changed genes (I) from pairwise comparisons of vehicle versus TM- or alprostadil-treated SKPs. The 23 overlapping genes in (I) are shown underneath. (J and K) Gene ontology (GO) enrichment analysis for gene categories that were significantly different in the comparisons of vehicle (Ctrl) versus TM- or alprostadil-treated SKPs showing highly significant enrichment for categories involving cell proliferation (J) and the MAP kinase (MAPK) pathway (K). See also Figure S2 and Tables S1, S2, S3, S4, S5, S6, S7, S8 and S9.

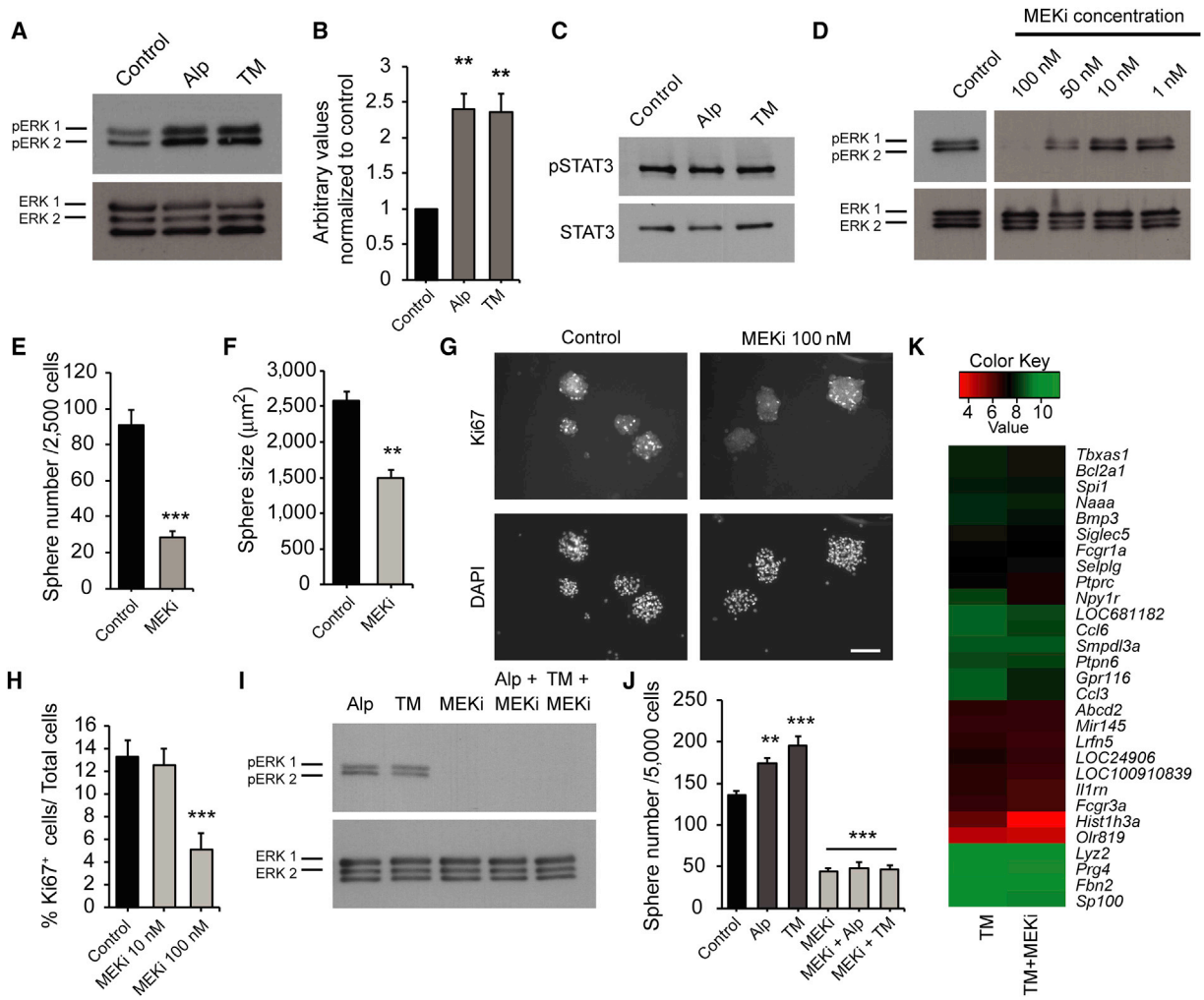

Figure 4. Signaling via the MEK-ERK Pathway Is Necessary for Basal and Drug-Induced SKPs Self-Renewal

(A–C) SKPs were treated with alprostadil (Alp), TM, or vehicle (Control) for 10 min, and lysates probed on western blots with anti-phosphorylated ERK1/2 T202/Y204 (pERK) (A) or anti-phosphorylated STAT3 (C) and reprobed for total ERK1/2 or total STAT3. (B) shows quantification by scanning densitometry of three experiments as in (A), where pERK was normalized to total ERK1/2.

(D) Western blot of SKPs treated with varying concentrations of trametinib (MEKi) or DMSO (Control) for 30 min, probed for pERK1/2 and reprobed for total ERK1/2.

(E and F) Number (E) and size (F) of SKP spheres generated in clonal methylcellulose assays from secondary neonatal rat SKPs grown 14 days in 100 nM trametinib or DMSO.

(G and H) Secondary rat SKPs were cultured for 4 days, and 10 or 100 nM trametinib added for 2 more days. (G) shows spheres immunostained for Ki67 (top) and counterstained with DAPI (bottom). (H) shows the percentage of Ki67-positive cells. Scale bar represents 100 μm.

(I) Western blot of SKPs treated with 100 nM trametinib for 30 min and coincidently stimulated with 100 nM alprostadil or TM for the final 10 min, probed for pERK1/2, and reprobed for total ERK1/2.

(J) Number of rat SKP spheres generated over 7 days in 100 nM alprostadil or TM with or without 100 nM trametinib.

(K) Heatmap comparing microarray data for three independent preparations of dissociated rat SKPs cultured for 24 hr in TM with or without trametinib, focusing on 29 of the top 50 genes that were altered by TM relative to control (see Figure 3), and that were significantly normalized by MEK inhibition. The heatmap shows the average of the raw expression (log_2) data for probesets that differed by $p < 0.01$ (unadjusted). In all cases, results are pooled from at least three independent experiments.

Error bars indicate SEM, and $^{**}p < 0.01$, $^{***}p < 0.001$, one-way ANOVA with multiple comparison post hoc tests, except (E and F), which were analyzed by Student's t test.

on a single intracellular pathway to enhance SKP self-renewal.

How do SKP self-renewal drugs promote skin repair? We previously showed that SKPs arise from, and are similar to, endogenous dermal precursors, and that transplantation of either population led to dermal reconstitution, dermal repair, and hair follicle morphogenesis (Biernaskie et al., 2009). We therefore propose that alprostadil and TM enhance skin repair by promoting proliferation and self-renewal of endogenous dermal precursors. Support for this idea comes from the data showing that SKPs isolated from drug-treated regenerating skin displayed a long-term increase in self-renewal. We suggest that alprostadil and TM enhanced the self-renewal and numbers of dermal precursors in vivo, and that this resulted in an increase in SKP sphere formation in culture. Precedent for this idea comes from studies where transient embryonic exposure to IL-6 led to an increase in adult forebrain neural precursors in vivo, and a persistent increase in sphere formation when these adult precursors were cultured (Gallagher et al., 2013). However, while our findings suggest that activation of dermal precursors underlies the enhanced skin repair, they do not exclude the possibility that alprostadil and/or TM also regulate other endogenous cells to promote wound healing.

Chronic skin wounds are a major medical problem (Eming et al., 2014), and there is a paucity of safe and effective approaches for promoting wound healing. Our findings suggest that targeting endogenous dermal precursors by repurposing of drugs already known to be safe in humans provides a new therapeutic approach for this largely unmet medical need.

EXPERIMENTAL PROCEDURES

Animals

This study was approved by the Hospital for Sick Children Animal Care Committee, in accordance with CCAC guidelines. Sprague-Dawley rats were purchased from Charles River. Punch wounds were performed on 9-month-old C57/Bl6 mice as described in the Supplemental Experimental Procedures (Biernaskie et al., 2009; Johnston et al., 2013). 100 μl of drugs or vehicle were applied topically around the wound or on uninjured shaved skin daily for 7–9 days, as indicated.

Cell Cultures

Neonatal rat SKPs were cultured from dorsal skin as previously described (Biernaskie et al., 2009; Fernandes et al., 2004) and in the Supplemental Experimental Procedures. For human SKPs, anonymized foreskin tissue from voluntary circumcisions was obtained with approval of the Research Ethics Board of the Hospital for Sick Children, and grown as described (Toma et al., 2005; Krause et al., 2014) and in the Supplemental Experimental Procedures. NIH 3T3 cells were grown as described in the Supplemental Experimental Procedures.

Drug Composition and Reagents

Drugs were reconstituted in DMSO (Sigma) at 50 mM for culture studies, and at 100 μM in propylene glycol-ethanol-water (40%:20%:40%) for topical application. All drugs were obtained from Sigma except latanoprost (Cayman Chemical) and trametinib (MedChemexpress).

SKP Screens

Screens using alamarBlue were performed as previously described (Smith et al., 2010) and in the Supplemental Experimental Procedures.

Sphere Formation Assays

Unless otherwise indicated, secondary or tertiary rat or human SKP spheres were seeded at 3,000–5,000 cells/well in 96-well plates, and compounds were added upon plating and at 3 days with fresh medium. At 7 days, cells were fixed, nuclei were stained with Hoechst 33258, sphere numbers were counted manually, and size was determined using Northern Eclipse software. For clonal sphere assays, SKPs were plated at 2,500 cells/ml in medium containing 1.6% methylcellulose and cultured for 14 days, as previously (Jinno et al., 2010; Biernaskie et al., 2009), with compounds added on days 1, 4, 8, and 12.

Tissue Preparation and Morphometric Analyses

Morphometric analyses were performed on paraffin-embedded sections, as described previously (Johnston et al., 2013) and in the Supplemental Experimental Procedures. Ki67-positive cells or CD31-positive blood vessels were determined from five representative 150-μm^2 fields randomly distributed over the leading edge of the regenerating dermis bordering the new epithelium, using Northern Eclipse software (Empix). All morphometric analyses were performed in a blinded manner. Antibodies are described in the Supplemental Experimental Procedures.

Western Blot Analysis

Secondary SKP spheres were dissociated and seeded at 10^6 cells/well in 6-well plates (Costar), cultured for 24 hr, treated as indicated, and analyzed on western blots as described (Naska et al., 2010). Densitometry was performed after subtracting the background using ImageJ software. Antibodies are described in the Supplemental Experimental Procedures.

Microarray Analysis

For microarrays of neonatal rat SKPs, secondary spheres were dissociated, treated with 100 nM drugs for 24 hr. For in vivo drug treatments, secondary SKP spheres were generated from drug-treated murine skin in medium without additional drugs. In both cases, RNA was isolated using the RiboPure Kit (Ambion by Life Technologies) and quality assessed by an Agilent BioAnalyzer. cDNA was generated with the Ambion Whole Transcript Expression Kit (Applied Biosystems) and was hybridized to the Affymetrix GeneChip Mouse Gene 2.0 ST or Rat Gene 2.0 ST arrays. The hybridized microarray image was scanned with the GeneChip Scanner 3000 7G (Affymetrix). Raw probe intensity

values were background corrected, normalized with quantile normalization, transformed into the $\log_2$ scale, and summarized into probesets with the Robust Multichip Analysis algorithm using the Oligo bioconductor package in R (Carvalho and Irizarry, 2010). For calculation of differential gene expression, the limma bioconductor package was used to calculate Bayesian statistics. In these analyses, any annotated gene with an expression change of $p < 0.01$ was considered statistically significant. For the hierarchical clustering and heatmap analysis, all the genes with $p < 0.01$ when comparing the injured skin and the alprostadil groups were used to perform the cluster and heatmap analysis on all groups using the heatmap.2 function of the gplots package in R. In this case, the complete linkage method of a Euclidian distance matrix was used to perform the cluster analysis. For acutely treated rat SKPs, heatmaps were produced by averaging $\log_2$ expression data for the three replicates for the appropriate groups and these data were displayed using the heatmap.2 function as described above. GO analysis was performed using the GOstats bioconductor package in R. The gene universe in this analysis was all of the mapped keys in the org.Mm.egGO and org.Ra.egGO databases for the Mouse Gene 2.0 ST and Rat Gene 2.0 ST arrays, respectively, while the differentially expressed genes (computed as described above) served as the enrichment samples. The threshold p value in the GO analysis was set at $p < 0.001$.

Statistical Analysis

Except for microarrays, data were expressed as the mean plus or minus the SEM and were tested for statistical significance with one-way ANOVA plus Dunnett's, Newman-Keuls', or Tukey's post hoc multiple comparison tests, unless otherwise indicated. All studies were performed with at least three independent biological replicates.

ACCESSION NUMBERS

Microarray data have been submitted to the NCBI GEO database under the accession number GEO: GSE73329.

SUPPLEMENTAL INFORMATION

Supplemental Information includes Supplemental Experimental Procedures, two figures, and nine tables and can be found with this article online at http://dx.doi.org/10.1016/j.stemcr.2015.12.002.

AUTHOR CONTRIBUTIONS

S.N. designed, performed, and analyzed many experiments and co-wrote the paper, S.A.Y. performed the microarray analyses and co-wrote the paper, A.P.W.J. performed many experiments and co-wrote the paper, S.P. participated in many of the experiments, M.V.S. assisted with the delivery formulation and some data interpretation, K.M.S. and M.P. validated the hits, K.M.S. and A.D. designed and performed screens, and F.D.M. and D.R.K. conceptualized the experiments, analyzed the data, and co-wrote the manuscript. All authors read the manuscript.

ACKNOWLEDGMENTS

This work was funded by CIHR grant MOP-64211 to F.D.M. and a Canadian Stem Cell Network Global Research grant to F.D.M. and D.R.K. S.A.Y. is funded by an Ontario Stem Cell Initiative fellowship. F.D.M. and D.R.K. hold Canada Research Chairs, and F.D.M. is an HHMI Senior International Research Scholar. We thank Darius Bagli for providing the human foreskin tissue, Tatiana Kroupnik, Natalie Grinshtein, Anastassia Voronova, and Guang Yang for advice and assistance.

Received: March 31, 2015
Revised: December 1, 2015
Accepted: December 1, 2015
Published: December 24, 2015

REFERENCES

Biernaskie, J., Paris, M., Morozova, O., Fagan, B.M., Marra, M., Pevny, L., and Miller, F.D. (2009). SKPs derive from hair follicle precursors and exhibit properties of adult dermal stem cells. Cell Stem Cell *5*, 610–623.

Boitano, A.E., Wang, J., Romeo, R., Bouchez, L.C., Parker, A.E., Sutton, S.E., Walker, J.R., Flaveny, C.A., Perdew, G.H., Denison, M.S., et al. (2010). Aryl hydrocarbon receptor antagonists promote the expansion of human hematopoietic stem cells. Science *329*, 1345–1348.

Breyer, R.M., Bagdassarian, C.K., Myers, S.A., and Breyer, M.D. (2001). Prostanoid receptors: subtypes and signaling. Annu. Rev. Pharmacol. Toxicol. *41*, 661–690.

Calderón-Montaño, J.M., Burgos-Morón, E., Pérez-Guerrero, C., and López-Lázaro, M. (2011). A review on the dietary flavonoid kaempferol. Mini Rev. Med. Chem. *11*, 298–344.

Carvalho, B.S., and Irizarry, R.A. (2010). A framework for oligonucleotide microarray preprocessing. Bioinformatics *26*, 2363–2367.

Dadwal, P., Mahmud, N., Sinai, L., Azimi, A., Fatt, M., Wondisford, F.E., Miller, F.D., and Morshead, C.M. (2015). Activating endogenous neural precursor cells using metformin leads to neural repair and functional recovery in a model of childhood brain injury. Stem Cell Rep. *5*, 166–173.

Delvaux, M., and Wingate, D. (1997). Trimebutine: mechanism of action, effects on gastrointestinal function and clinical results. J. Int. Med. Res. *25*, 225–246.

Eming, S.A., Martin, P., and Tomic-Canic, M. (2014). Wound repair and regeneration: mechanisms, signaling, and translation. Sci. Transl. Med. *6*, 265sr6.

Falcon, S., and Gentleman, R. (2007). Using GOstats to test gene lists for GO term association. Bioinformatics *23*, 257–258.

Fernandes, K.J.L., McKenzie, I.A., Mill, P., Smith, K.M., Akhavan, M., Barnabé-Heider, F., Biernaskie, J., Junek, A., Kobayashi, N.R., Toma, J.G., et al. (2004). A dermal niche for multipotent adult skin-derived precursor cells. Nat. Cell. Biol. *6*, 1082–1093.

Fisher, A.A. (1998). The safety of pramoxine hydrochloride when used as a topical (surface) anesthetic. Cutis *62*, 122–123.

Gallagher, D., Norman, A.A., Woodard, C.L., Yang, G., Gauthier-Fisher, A., Fujitani, M., Vessey, J.P., Cancino, G.I., Sachewsky, N.,

Woltjen, K., et al. (2013). Transient maternal IL-6 mediates long-lasting changes in neural stem cell pools by deregulating an endogenous self-renewal pathway. Cell Stem Cell *13*, 564–576.

Gilmartin, A.G., Bleam, M.R., Groy, A., Moss, K.G., Minthorn, E.A., Kulkarni, S.G., Rominger, C.M., Erskine, S., Fisher, K.E., Yang, J., et al. (2011). GSK1120212 (JTP-74057) is an inhibitor of MEK activity and activation with favorable pharmacokinetic properties for sustained in vivo pathway inhibition. Clin. Cancer Res. *17*, 989–1000.

Gotti, C., Balestra, B., Moretti, M., Rovati, G.E., Maggi, L., Rossoni, G., Berti, F., Villa, L., Pallavicini, M., and Clementi, F. (1998). 4-Oxystilbene compounds are selective ligands for neuronal nicotinic alphaBungarotoxin receptors. Br. J. Pharmacol. *124*, 1197–1206.

Gutstein, H.B., Rubie, E.A., Mansour, A., Akil, H., and Woodgett, J.R. (1997). Opioid effects on mitogen-activated protein kinase signaling cascades. Anesthesiology *87*, 1118–1126.

Hanchanale, V., and Eardley, I. (2014). Alprostadil for the treatment of impotence. Expert Opin. Pharmacother. *15*, 421–428.

Hsu, Y.-C., Li, L., and Fuchs, E. (2014). Emerging interactions between skin stem cells and their niches. Nat. Med. *20*, 847–856.

Jinno, H., Morozova, O., Jones, K.L., Biernaskie, J.A., Paris, M., Hosokawa, R., Rudnicki, M.A., Chai, Y., Rossi, F., Marra, M.A., and Miller, F.D. (2010). Convergent genesis of an adult neural crest-like dermal stem cell from distinct developmental origins. Stem Cells *28*, 2027–2040.

Johnston, A.P.W., Naska, S., Jones, K., Jinno, H., Kaplan, D.R., and Miller, F.D. (2013). Sox2-mediated regulation of adult neural crest precursors and skin repair. Stem Cell Rep. *1*, 38–45.

Kaneto, H., Takahashi, M., and Watanabe, J. (1990). The opioid receptor selectivity for trimebutine in isolated tissues experiments and receptor binding studies. J. Pharmacobiodyn. *13*, 448–453.

Krause, M.P., Dworski, S., Feinberg, K., Jones, K., Johnston, A.P.W., Paul, S., Paris, M., Peles, E., Bagli, D., Forrest, C.R., et al. (2014). Direct genesis of functional rodent and human Schwann cells from skin mesenchymal precursors. Stem Cell Rep. *3*, 85–100.

McKenzie, I.A., Biernaskie, J., Toma, J.G., Midha, R., and Miller, F.D. (2006). Skin-derived precursors generate myelinating Schwann cells for the injured and dysmyelinated nervous system. J. Neurosci. *26*, 6651–6660.

Miller, F.D., and Kaplan, D.R. (2012). Mobilizing endogenous stem cells for repair and regeneration: are we there yet? Cell Stem Cell *10*, 650–652.

Naska, S., Lin, D.C., Miller, F.D., and Kaplan, D.R. (2010). p75NTR is an obligate signaling receptor required for cues that cause sympathetic neuron growth cone collapse. Mol. Cell. Neurosci. *45*, 108–120.

Ritchie, M.E., Phipson, B., Wu, D., Hu, Y., Law, C.W., Shi, W., and Smyth, G.K. (2015). limma powers differential expression analyses for RNA-sequencing and microarray studies. Nucleic Acids Res. *43*, e47.

Sasaki, S., Hozumi, Y., and Kondo, S. (2005). Influence of prostaglandin F2alpha and its analogues on hair regrowth and follicular melanogenesis in a murine model. Exp. Dermatol. *14*, 323–328.

Smith, K.M., Datti, A., Fujitani, M., Grinshtein, N., Zhang, L., Morozova, O., Blakely, K.M., Rotenberg, S.A., Hansford, L.M., Miller, F.D., et al. (2010). Selective targeting of neuroblastoma tumour-initiating cells by compounds identified in stem cell-based small molecule screens. EMBO Mol. Med. *2*, 371–384.

Tata, S., Flynn, G.L., and Weiner, N.D. (1995). Penetration of minoxidil from ethanol/propylene glycol solutions: effect of application volume and occlusion. J. Pharm. Sci. *84*, 688–691.

Toma, J.G., Akhavan, M., Fernandes, K.J., Barnabé-Heider, F., Sadikot, A., Kaplan, D.R., and Miller, F.D. (2001). Isolation of multipotent adult stem cells from the dermis of mammalian skin. Nat. Cell Biol. *3*, 778–784.

Toma, J.G., McKenzie, I.A., Bagli, D., and Miller, F.D. (2005). Isolation and characterization of multipotent skin-derived precursors from human skin. Stem Cells *23*, 727–737.

Wang, J., Gallagher, D., DeVito, L.M., Cancino, G.I., Tsui, D., He, L., Keller, G.M., Frankland, P.W., Kaplan, D.R., and Miller, F.D. (2012). Metformin activates an atypical PKC-CBP pathway to promote neurogenesis and enhance spatial memory formation. Cell Stem Cell *11*, 23–35.

Yu, L., Wu, W.K.K., Li, Z.J., Wong, H.P.S., Tai, E.K.K., Li, H.T., Wu, Y.C., and Cho, C.H. (2008). E series of prostaglandin receptor 2-mediated activation of extracellular signal-regulated kinase/activator protein-1 signaling is required for the mitogenic action of prostaglandin E2 in esophageal squamous-cell carcinoma. J. Pharmacol. Exp. Ther. *327*, 258–267.

Stem Cell Reports, Volume *6*

Supplemental Information

Identification of Drugs that Regulate Dermal Stem Cells and Enhance Skin Repair

Sibel Naska, Scott A. Yuzwa, Adam P.W. Johnston, Smitha Paul, Kristen M. Smith, Maryline Paris, Michael V. Sefton, Alessandro Datti, Freda D. Miller, and David R. Kaplan

Supplemental Information

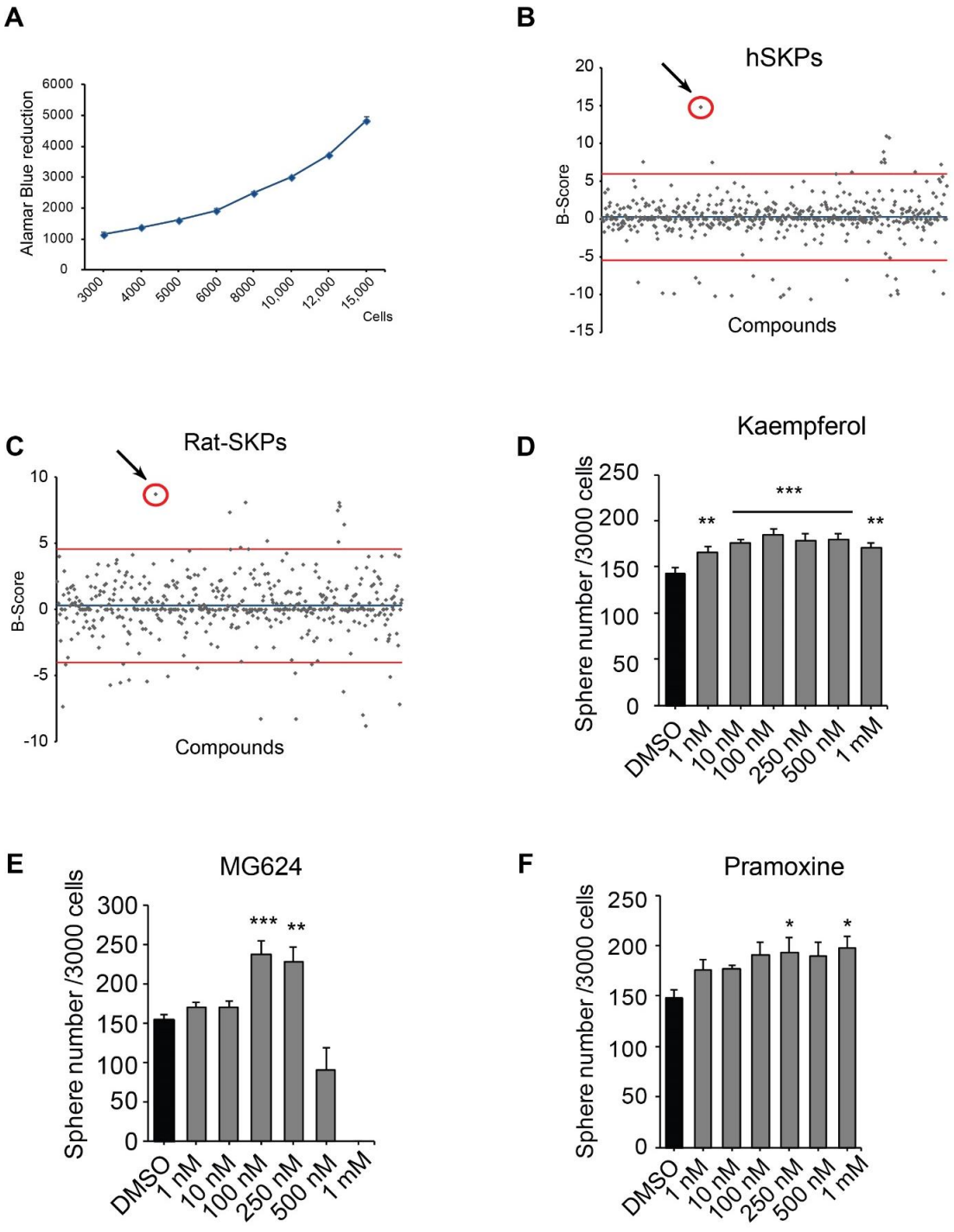

Supplemental Figure S1: ***Identification of compounds that enhance self-renewal and proliferation of cultured SKPs, Related to Figure 1.*** (A) Dissociated secondary neonatal rat

SKPs were robotically plated at 3,000 to 15,000 cells/well in 96 well plates, alamarBlue® was added after 30 hours and the plates were analyzed after an additional 24 hours. The graph shows the fluorescence signal caused by reduction of alamarBlue® (with the medium value subtracted) in wells with increasing numbers of cells. (B,C) Representative B-Score plots from the NIH collection library screened against human (B) or rat (C) SKPs. The red lines indicate three standard deviations from the mean. Compounds with B-scores greater than three standard deviations were considered primary hits. Arrows indicate the hit compound TM that was identified in both human (B) and rat (C) SKP screens. (D-F) Number of SKP spheres generated from secondary human SKPs grown for 7 days in varying concentrations of kaempferol (D), MG-624 (E) or pramoxine (F). Controls were treated with DMSO alone. Results are pooled from at least 3 independent experiments with 3 different human SKP lines ($n \geq 3$ wells each). Error bars indicate SEM, and in all cases *$p<0.05$, **$p<0.01$, ***$p<0.001$, one-way ANOVA with multiple comparison post-hoc tests.

A

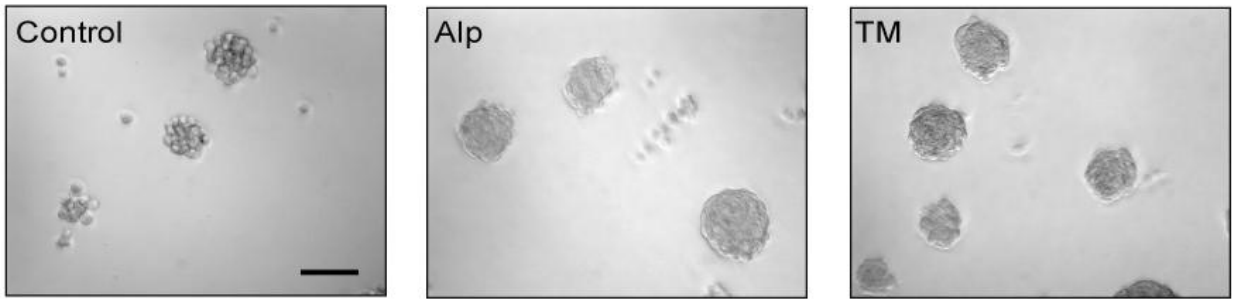

B

Overlapping Genes:

uck2; slc44a1; 9430024e24rik; trim34a; gm20257; krtap9-1; cox1; tuba1b; gm10517; vstm2l; oxct1; gm10684; 2310079g19rik; 4930590j08rik; mdh1b; tmed11; olfr898; htatsf1; foxj1; gm8579; paqr9

Supplemental Figure S2: ***In vivo aprostadil and TM treatment enhance SKP sphere formation and induce overlapping differentially expressed genes, Related to Figure 3.*** (A) Representative images of cultured secondary SKP spheres generated from injured skin treated with alprostadil (Alp), TM or vehicle (Control) for 7 days. Scale bar = 100 μm. (B) mRNA from secondary SKP spheres generated as in (A) were analyzed on Affymetrix GeneChip Mouse Gene 2.0 ST arrays. The list indicates overlapping genes that differ by $p < 0.01$ (unadjusted) in pairwise comparisons of vehicle (Control) versus TM or alprostadil-treated injured skin.

Supplemental Table S1: ***Differentially expressed genes in secondary SKP spheres generated from injured skin treated with vehicle versus alprostadil, Related to Figure 3.*** Secondary SKP spheres were generated from the skin of 9 month old mice that had received punch wounds and were treated topically with vehicle or alprostadil for 7 days. mRNA from these SKP spheres was analyzed on Affymetrix GeneChip Mouse Gene 2.0 ST arrays, and differentially expressed genes were determined using the limma bioconductor package at the probeset level to generate $\log_2$ fold-change (shown here as inverse $\log_2$ fold-change) and moderated t-statistics and comparing vehicle versus alprostadil. Differentially expressed genes were annotated using the mogene20sttranscriptcluster.db bioconductor annotation package to annotate the gene symbol and description shown here. Differentially expressed genes with known annotations and p-values < 0.01 were included.

Supplemental Table S2*: Differentially expressed genes in secondary SKP spheres generated from injured skin treated with vehicle versus TM, Related to Figure 3.* Secondary SKP spheres were generated from the skin of 9 month old mice that had received punch wounds and were treated topically with vehicle or TM for 7 days. mRNA from these SKP spheres was analyzed on Affymetrix GeneChip Mouse Gene 2.0 ST arrays, and differentially expressed genes were determined using the limma bioconductor package at the probeset level to generate $\log_2$ fold-change (shown here as inverse $\log_2$ fold-change) and moderated t-statistics and comparing vehicle versus TM. Differentially expressed genes were annotated using the mogene20sttranscriptcluster.db bioconductor annotation package to annotate the gene symbol and description shown here. Differentially expressed genes with known annotations and p-values < 0.01 were included.

Supplemental Table S3*: Differentially expressed genes in neonatal rat SKPs treated for 24 hours with alprostadil, Related to Figure 3:* Three independent preparations of primary neonatal rat SKPs were dissociated and cultured for 24 hours in alprostadil or vehicle, and mRNA was isolated and analyzed on Affymetrix GeneChip Rat Gene 2.0 ST arrays. Differentially expressed genes were determined for the pairwise comparisons between vehicle and alprostadil-treated SKPs, computed using the limma bioconductor package at the probeset level to generate $\log_2$ fold-change (shown here as inverse $\log_2$ fold-change) and moderated t-statistics. Differentially expressed genes were annotated using the ragene20sttranscriptcluster.db bioconductor annotation package to annotate the gene symbol and description shown here. Differentially expressed genes with known annotations and p-values < 0.01 are included.

Supplemental Table S4*: Differentially expressed genes in neonatal rat SKPs treated for 24 hours with TM, Related to Figure 3:* Three independent preparations of primary neonatal rat SKPs were dissociated and cultured for 24 hours in TM, or vehicle, and mRNA was isolated and analyzed on Affymetrix GeneChip Rat Gene 2.0 ST arrays. Differentially expressed genes were determined for the pairwise comparisons between vehicle and TM treated SKPs, computed using the limma bioconductor package at the probeset level to generate $\log_2$ fold-change (shown here as inverse $\log_2$ fold-change) and moderated t-statistics. Differentially expressed genes were annotated using the ragene20sttranscriptcluster.db bioconductor annotation package to annotate the gene symbol and description shown here. Differentially expressed genes with known annotations and p-values < 0.01 are included.

Supplemental Table S5*: Overlapping differentially expressed genes (p < 0.01) comparing neonatal rat SKPs treated for 24 hours with alprostadil or TM, Related to Figure 3.*

Gene symbols: *loc100910839, lyz2, ccl6, klra17, siglec5, myo1f, lcp1, scimp, rgs1, ptprc, smpdl3a, loc24906, loc681325, ptk2b, prg4, rgd1561143, rspo3, bmp3, rgd1561730, cidec, adipoq, gpd1, csf1r, gldn, cpa3, cd37, car3, cfh, ccl9, bcl2a1, fcgr2a, spi1, parvg, lcp2, fam105a, loc681182, igsf6, slc25a43, tbxas1, ncf1, cd53, clec4a3, mmp11, lipg, gpr116, itgb2, sirpa, cttnbp2, kcnj2, lrrc15, sema4a, tnfsf13, cd74, lilrb4, selplg, trpv2, ptpn6, tmem176a, rbp4, fgr, bmp7, acsl1, lyn, itgal, tfpi2, alox5, cfp, sla, nfam1, ucp2, npy1r, sort1, il18, dock8, was, aqp7, fbn2, prelp, emr4, gmfg, tfec, fabp4, nnat, cd180, fcer1g, rgs18, des, gpr65, pla2g7, retn, nckap1l, kcnn4, fcgr1a, siglec10, s100b, tmem2, myo1g, ass1, sfrp1, tusc5, lipa, siglec8, tlr7, prss23, rpp25, dock10, inhba, syk, slc6a6, hpse2, ar, clec4a1, chrna5, cidea, frmpd4, plekha6, gpnmb, c3, ccl22, qprt, hist1h3a, sh2d1b, sertm1, bmp5, lrfn5, prdm6, cdc6, serpina3n, tacr3, akap6, col14a1, tyrobp, scd1, serpinb1a, gpr133, pck1, nefl, ccl3, atp1b1, ces1a, tll1, lrrn3, arhgdib, ptprn, dgat2, slc6a12, fcgr3a, gabarapl1, aspn, vav1, tmem176b, dpep1, ifi30, creg1, loc688459, stxbp2, itga8, c1qb, naaa, scn7a, ceacam1, gm2a, myo1d, epha4, ptpro, sult1a1, megf10, gpx3, rbm47, epha7, ptgs2, tnfrsf26, cfd, aspa, kcnn3, tmem100, prl3d4, sdc3, itgam, ddah1, clec5a, clec4e, pla2g2d, npr3, has1, msr1, epha3, cpxm1, lcn2, elmo1, mfap5, cyp4b1, sox4, pik3r5, fermt3, mgst1, march1, nos1, mir323, dapp1, gas6, clec4d, gpc3, b3galt1, slitrk5, mir223, cst6, fam111a, gramd1b, ptn, mir493, prdx5, chaf1b, il1rn, mctp2, rtp3, tnfaip8l2, sox2, unc93b1, bin2, akap5, abi3bp, cytip, dhrs3, n4bp2, coro1a, mirlet7c-1, abhd2, il1b, il33, cmklr1, treml4, nlrc4, drp2, pdia5, abcd2, apobec1, capn6, ptger3, rgd1566085, aoah, abcg1, mcemp1, cdh13, ebpl, tf, myo1e, crabp1, plbd1, foxp1, ms4a7, jam2, atp8b1, mdga2, h19, crip2, rgd1305089, dgkb, tmem35, lonrf2, cd302, fst, b3gnt7, sp100, zdhhc14, shc4, nqo2, parm1, hpgds, cyp26b1, olr1051, napsa, rac2, plin1, il20rb, diras2, krt31, slc7a1, fli1, dtl, sez6l, fxyd1, ms4a4a, slco2a1, steap1, inpp5d, ablim3, vldlr, cdo1, cdc42ep3, lrrc25, cyp4f39, rgd1309362, shc3*

Overlapping differentially expressed genes from the pairwise comparisons of neonatal rat SKPs treated with vehicle versus alprostadil or TM, as shown in Suppl. Tables S3 and S4, and as computed using the limma bioconductor package at the probeset level to generate $\log_2$ fold-change (shown here as inverse $\log_2$ fold-change) and moderated t-statistics. Differentially expressed genes were annotated using the ragene20sttranscriptcluster.db bioconductor annotation package.

Supplemental Table S6*: Top 50 differentially expressed genes in neonatal rat SKPs treated for 24 hours with alprostadil, Related to Figure 3.*

Gene Symbol	Description	Fold-Change	P-value (moderated t-statistic)
LOC100910839	leucine zipper protein 2-like	1.001921	3.18E-05
Lyz2	lysozyme 2	1.041509	5.20E-05
Il6	interleukin 6	6.07487	6.07E-05
Ccl6	chemokine (C-C motif) ligand 6	1.794098	6.35E-05
Klra17	killer cell lectin-like receptor, subfamily A, member 17	0.961245	6.87E-05
Siglec5	sialic acid binding Ig-like lectin 5	1.08744	8.78E-05
Myo1f	myosin IF	0.71582	8.79E-05
Lcp1	lymphocyte cytosolic protein 1	0.835355	8.99E-05
Scimp	SLP adaptor and CSK interacting membrane protein	1.306032	0.000104
Rgs1	regulator of G-protein signaling 1	1.169478	0.000113
Ptprc	protein tyrosine phosphatase, receptor type, C	0.93395	0.000132
Cxcl13	chemokine (C-X-C motif) ligand 13	4.189169	0.000139
Smpdl3a	sphingomyelin phosphodiesterase, acid-like 3A	1.173385	0.000144
LOC24906	RoBo-1	1.835212	0.000145
LOC681325	hypothetical protein LOC681325	1.154336	0.000156
Ptk2b	protein tyrosine kinase 2 beta	1.013942	0.000173
Prg4	proteoglycan 4	1.167444	0.000178
Ccl12	chemokine (C-C motif) ligand 12	0.326009	0.000181
RGD1561143	similar to cell surface receptor FDFACT	1.009887	0.000185
Rspo3	R-spondin 3	1.649091	0.000185
Bmp3	bone morphogenetic protein 3	0.927272	0.000198
RGD1561730	similar to cell surface receptor FDFACT	1.184263	0.000207
Cidec	cell death-inducing DFFA-like effector c	0.826168	0.000221
Adipoq	adiponectin, C1Q and collagen domain containing	1.014716	0.000228
Gpd1	glycerol-3-phosphate dehydrogenase 1 (soluble)	0.908651	0.000256
Csf1r	colony stimulating factor 1 receptor	1.088615	0.000259
Gldn	gliomedin	0.896379	0.000262
Cpa3	carboxypeptidase A3, mast cell	0.925526	0.000265
Cd37	CD37 molecule	1.019646	0.00027
Car3	carbonic anhydrase 3	0.924688	0.00027
Cfh	complement factor H	0.713577	0.00029
Phlda1	pleckstrin homology-like domain, family A, member 1	2.12465	0.000292
Ccl9	chemokine (C-C motif) ligand 9	0.907055	0.000309
Bcl2a1	BCL2-related protein A1	0.965589	0.000313
Fcgr2a	Fc fragment of IgG, low affinity IIa, receptor	1.194083	0.000323
Spi1	Spi-1 proto-oncogene	0.952852	0.000349
Parvg	parvin, gamma	0.997287	0.000382
Lcp2	lymphocyte cytosolic protein 2	0.955288	0.000406
Fam105a	family with sequence similarity 105, member A	1.002798	0.000411
LOC681182	similar to paired immunoglobin-like type 2 receptor beta	1.129033	0.000411
Igsf6	immunoglobulin superfamily, member 6	1.34594	0.000411
Slc25a43	solute carrier family 25, member 43	0.954538	0.000421
Tbxas1	thromboxane A synthase 1, platelet	1.070738	0.000431
Ncf1	neutrophil cytosolic factor 1	0.903086	0.000433
Cd53	Cd53 molecule	1.342827	0.000435
Hs3st1	heparan sulfate (glucosamine) 3-O-sulfotransferase 1	1.997368	0.000456
Clec4a3	C-type lectin domain family 4, member A3	0.596755	0.000458
Mmp11	matrix metallopeptidase 11	0.855951	0.00046
Slpi	secretory leukocyte peptidase inhibitor	1.494137	0.000472
Lipg	lipase, endothelial	0.972027	0.000486

Three independent preparations of primary neonatal rat SKPs were dissociated and cultured for 24 hours in alprostadil, or vehicle, and mRNA was isolated and analyzed on Affymetrix GeneChip Rat Gene 2.0 ST array. Shown here are the top 50 differentially expressed genes

(highest significance and known annotations) for the pairwise comparisons between vehicle and alprostadil treated SKPs, as computed using the limma bioconductor package at the probeset level to generate $\log_2$ fold-change (shown here as inverse $\log_2$ fold-change) and moderated t-statistics. Differentially expressed genes were annotated using the ragene20sttranscriptcluster.db bioconductor annotation package to annotate the gene symbol and description shown here.

Supplemental Table S7*: Top 50 differentially expressed genes in neonatal rat SKPs treated for 24 hours with TM, Related to Figure 3.*

Gene Symbol	Description	Fold-Change	P-value (moderated t-statistic)
Scimp	SLP adaptor and CSK interacting membrane protein	1.233397	4.00E-05
Ptprc	protein tyrosine phosphatase, receptor type, C	1.145283	4.63E-05
Siglec5	sialic acid binding Ig-like lectin 5	1.15008	5.18E-05
Fabp4	fatty acid binding protein 4, adipocyte	0.964711	8.74E-05
Clec4a3	C-type lectin domain family 4, member A3	0.916971	0.000114
Cidec	cell death-inducing DFFA-like effector c	1.024594	0.000122
Fam105a	family with sequence similarity 105, member A	1.071321	0.000126
Cpa3	carboxypeptidase A3, mast cell	0.779702	0.000173
LOC100910839	leucine zipper protein 2-like	1.109524	0.000179
Adipoq	adiponectin, C1Q and collagen domain containing	0.962054	0.000181
LOC681182	similar to paired immunoglobin-like type 2 receptor beta	1.049692	0.000206
Gpr133	G protein-coupled receptor 133	1.043488	0.000242
Acsl1	acyl-CoA synthetase long-chain family member 1	1.006802	0.000253
Selplg	selectin P ligand	1.089982	0.000254
Fcgr3a	Fc fragment of IgG, low affinity IIIa, receptor	1.053318	0.000266
Il1rn	interleukin 1 receptor antagonist	1.123454	0.00031
Naaa	N-acylethanolamine acid amidase	1.068007	0.000316
Bcl2a1	BCL2-related protein A1	0.943153	0.000333
Sema4a	sema domain, immunoglobulin domain (Ig), transmembrane domain (TM) and short cytoplasmic domain, (semaphorin) 4A	1.068099	0.000356
Smpdl3a	sphingomyelin phosphodiesterase, acid-like 3A	1.146783	0.000357
Ccl6	chemokine (C-C motif) ligand 6	1.187186	0.000366
Lrfn5	leucine rich repeat and fibronectin type III domain containing 5	0.991541	0.000387
Tbxas1	thromboxane A synthase 1, platelet	1.13564	0.000392
Bmp3	bone morphogenetic protein 3	1.02108	0.000413
Csf1r	colony stimulating factor 1 receptor	0.987028	0.000415
Hist1h3a	histone cluster 1, H3a	0.680929	0.000421
Il18	interleukin 18	0.865269	0.000426
Npy1r	neuropeptide Y receptor Y1	0.914961	0.000448
Fcgr1a	Fc fragment of IgG, high affinity Ia, receptor (CD64)	1.0427	0.000459
Cxcr1	chemokine (C-X-C motif) receptor 1	0.938585	0.000461
Abcd2	ATP-binding cassette, subfamily D (ALD), member 2	1.020682	0.000487
Gpd1	glycerol-3-phosphate dehydrogenase 1 (soluble)	0.914691	0.00049
Aoah	acyloxyacyl hydrolase (neutrophil)	1.077756	0.000492
Sp100	SP100 nuclear antigen	0.919426	0.000529
Rspo3	R-spondin 3	1.104077	0.000537
LOC24906	RoBo-1	0.953287	0.000543
Lyz2	lysozyme 2	1.075892	0.000555
Gpc3	glypican 3	0.941928	0.000557
Spi1	Spi-1 proto-oncogene	1.03597	0.000566
Olr1726	olfactory receptor 1726	0.64766	0.000581
Ccl3	chemokine (C-C motif) ligand 3	0.906386	0.000581
Mmp11	matrix metallopeptidase 11	1.015164	0.00059
Prg4	proteoglycan 4	0.97482	0.000591
Gpr116	G protein-coupled receptor 116	1.004721	0.000619
Pla2g7	phospholipase A2, group VII (platelet-activating factor acetylhydrolase, plasma)	1.000346	0.000627
Ptpn6	protein tyrosine phosphatase, non-receptor type 6	0.995589	0.000648
Mir145	microRNA 145	0.956693	0.000659
Fbn2	fibrillin 2	0.984266	0.000719
Mirlet7c-1	microRNA let-7c-1	0.846102	0.000731
Olr819	olfactory receptor 819	1.208596	0.000733

Three independent preparations of primary neonatal rat SKPs were dissociated and cultured for 24 hours in TM or vehicle, and mRNA was isolated and analyzed on Affymetrix GeneChip Rat

Gene 2.0 ST array. Shown here are the top 50 differentially expressed genes (highest significance and known annotations) for the pairwise comparisons between vehicle and TM-treated SKPs, as computed using the limma bioconductor package at the probeset level to generate $\log_2$ fold-change (shown here as inverse $\log_2$ fold-change) and moderated t-statistics. Differentially expressed genes were annotated using the ragene20sttranscriptcluster.db bioconductor annotation package to annotate the gene symbol and description shown here.

Supplemental Table S8*: Differentially expressed genes associated with GO terms for proliferation from neonatal rat SKPs treated for 24 hours with TM or alprostadil, Related to Figure 3.* Three independent preparations of primary neonatal rat SKPs were dissociated and cultured for 24 hours in alprostadil (Alp), TM or vehicle (Ctrl), and mRNA was isolated and analyzed on Affymetrix GeneChip Rat Gene 2.0 ST array. Gene-ontology (GO) enrichment analysis identified genes that were significantly different in the comparisons of vehicle versus TM or alprostadil-treated SKPs and that were associated with GO categories for cell proliferation (as shown in Fig. 3J). These genes are listed here. Some listed genes are associated with more than one category.

Supplemental Table S9: *Differentially expressed genes associated with GO terms for MAPK/ERK from neonatal rat SKPs treated for 24 hours with TM or alprostadil, Related to Figure 3.* Three independent preparations of primary neonatal rat SKPs were dissociated and cultured for 24 hours in alprostadil (Alp), TM or vehicle (Ctrl), and mRNA was isolated and analyzed on Affymetrix GeneChip Rat Gene 2.0 ST array. Gene-ontology (GO) enrichment analysis identified genes that were significantly different in the comparisons of vehicle versus TM or alprostadil-treated SKPs and that were associated with GO categories for MAPK/ERK (as shown in Fig. 3K). These genes are listed here. Some listed genes are associated with more than one category.

Supplemental Experimental Procedures

Preparation of SKP cultures. SKPs were isolated from the back skin of newborn Sprague-Dawley rat pups or from the back skin of 9 month old CD57/Bl6 mice. Skin was dissected and cut into 1-2 mm pieces and incubated in collagenase type XI (Sigma) for 30 min at 37°C. Samples were centrifuged, the supernatant was removed, and tissue pieces were resuspended in medium (DMEM/F12, 3:1 [Invitrogen] containing 1% penicillin/streptomycin [P/S]) and manually dissociated by pipetting. Cells were cultured at 50,000 cells/ml in SKPs basal growth medium (DMEM-F12, 3:1 and 40 ng/ml FGF2 [Peprotech], 20 ng/ml EGF [BD Biosciences], 2% B27 [Invitrogen], and 1 μg/ml fungizone [Invitrogen]) and allowed to form spheres. For human SKPs, anonymized foreskin tissue from voluntary circumcisions was cut into 4-6-mm pieces, and incubated in Liberase DH Research grade Dispase High (0.60 Wunsch U/ml; Roche Molecular Biochemicals) overnight at 4°C. Epidermis was manually removed and dermis was further cut into 1 mm pieces and incubated in Liberase for 30-40 min at 37°C. DNase I was added for 1 min, and 10% fetal bovine serum (FBS; Fisher Scientific) was added to inhibit the enzymes. The supernatant was removed, and tissue pieces were resuspended in medium (DMEM/F12, 3:1 [Invitrogen] containing1% penicillin/streptomycin [P/S]) and manually dissociated by pipetting. Once tissue was dissociated, the cell suspension was filtered through a 70-μm-cell strainer (BD Biosciences). The strained cell suspension was centrifuged at 1,000 rpm for 5 min, supernatant was aspirated, and cells were plated at a density of 50-100,000 cells/ml in SKPs basal growth medium. To generate secondary spheres, SKPs were digested in collagenase (1 mg/ml; type XI; Sigma) for 15-30 min at 37°C and then mechanically dissociated to single cells by pipetting. Medium (DMEM/F12) was added to inhibit the enzyme. Cells were centrifuged at 1,000 rpm for 5 min. Supernatant was removed and cells were passaged into 50% new growth medium and 50% of the same medium pre-conditioned by SKPs to generate secondary spheres. All experiments were done using secondary or tertiary spheres. For SKPs drug-screening assays, secondary or tertiary passage human or rat SKP spheres were dissociated and 3000 human or 5000 rat SKP cells were robotically seeded in each well of 96-well uncoated plates (Costar, Corning Life Sciences). Compounds (1-5 μM) were added in singlet and plates were incubated in SKPs basal growth medium plus 50% of the same medium pre-conditioned by

SKPs. AlamarBlue dye (Life Technologies) was added after 30 hrs, and its reduction to a fluorescent compound was measured after another 24 hrs.

NIH 3T3 cultures. NIH 3T3 cells were grown in DMEM containing 10% FBS and 1% penicillin/streptomycin and plated at a density of 25,000 cells / cm^2. The following day, alprostadil and TM were added to the NIH 3T3 cultures at 100 nM and 24 hours later cells were fixed and immunostained for Ki67.

Skin wounding and morphometric analysis. To induce skin wounds 9 month old mice were anesthetized, the dorsal hair was shaved and the exposed skin was cleaned with ethanol. Two 6 mm diameter full thickness excisional wounds were performed on each side of the dorsal midline using a biopsy punch (Miltex). For consistency, only one wound on the right dorsal side of each mouse was used for analysis (punch from outside to inside skin). Wounds were left uncovered and mice were given Anafen for analgesia and housed individually. To quantify wound size, digital photographs (Canon) were taken at day 0, 3, 7 and 9 post wounding. A ruler was used to calibrate the images and the wound margins were manually outlined using Northern Eclipse software (Empix). The wound closure rate was calculated as a percentage of the wound size on the day of surgery, using the following formula: % wound closure = $(area_i\text{-}area_f) \times 100/area_i$ where $area_i$ is the initial wound area at day 0 and $area_f$ is the final area (Martin et al., 2010). At 9 days post-injury, mice were sacrificed, and the wound bed was excised and fixed in 10% formalin and embedded in paraffin. Wounds were bisected in a caudocranial direction and serial sections from the central portion of the wound were stained with hematoxylin and eosin and used for histology. Sections were scanned using a 20x/0.75 lens (Zeiss Mirax Scan) and were stitched together using the Mirax Scan software. Morphometric analysis were performed as described previously (Johnston et al., 2013; Martin et al., 2010), using Northern Eclipse software (Empix). Epithelial gap was measured as the distance between the new epithelial tongues. Wound width was measured as the distance between the wound margins which were defined by the last hair follicles. Finally, dermal tissue thickness was given a score of 1, 2 or 3 for very thin, moderate or thick dermis, respectively.

Antibodies. For immunohistochemistry of skin sections primary antibodies were rabbit anti-Ki67 (1:100; LabVision) or rabbit anti-CD31 (1:100; Abcam) followed by a biotin-conjugated goat anti-rabbit secondary, and the ABC-DAB detection kit (Vector Laboratory). For western blotting, primary antibodies were rabbit anti-pERK1/2 T202/Y204 (1:2000, Cell Signaling), rabbit anti-ERK1/2 (1:10,0000, Santa Cruz), rabbit anti-pSTAT3 Tyr705 (1:1000, Cell Signaling) and mouse anti-STAT3 (1:1000, Cell Signaling) and secondary antibodies were HRP-conjugated goat anti-mouse (1:10,000; Millipore) or goat anti-rabbit (1:10,000). Protein was detected using the ECL kit (GE Healthcare)

Supplemental References

Martin, D.C., Semple, J.L., and Sefton, M.V. (2010). Poly(methacrylic acid-co-methyl methacrylate) beads promote vascularization and wound repair in diabetic mice. J. Biomed. Mater. Res. A *93*, 484–492.